Journal of Applied Spectroscopy, Vol. 75, No. 6, 2008

EFFECT OF METALLIC NANOPARTICLE SIZES ON THE LOCAL FIELD NEAR THEIR SURFACE

R. A. Dynich and A. N. Ponyavina*

UDC 535.343:539.184:541.1

We have used numerical calculations based on Mie theory to analyze the near field distribution patterns for 4–150 nm spherical silver nanoparticles (nanospheres). We have shown that as the nanoparticle sizes increase, the region where "hot spots" are concentrated is shifted to the forward hemisphere. We have observed a nonmonotonic dependence of the maximum attainable local field enhancement factor on the size of the silver nanospheres. We have determined a correlation between the optimal nanosphere size for the maximum attainable local field enhancement factor and the optical absorption efficiency factor. We have established a nonmonotonic dependence of the optimal size of the nanoparticles and the maximum attainable local field enhancement factor on the refractive index of the surrounding medium.

Key words: *nanostructure, surface plasmon resonance, near field characteristics, local field enhancement.*

Introduction. Materials containing nanoparticles of noble metals are being actively studied today because of their important properties connected with formation of surface plasmon resonance (SPR) absorption bands in the visible region of the spectrum and substantial enhancement of local fields near the surface of the metallic nanoparticles ("hot spots"). Resonance enhancement of local characteristics of the optical field has a considerable effect on formation of linear and nonlinear optical properties of aggregated nanodispersed structures, and the extent to which these resonances appear can be effectively controlled by varying the topological and morphological parameters of the nanocomposites. Significant local field enhancement and its considerable nonuniformity are important factors leading to the appearance of "surface-enhanced" optical effects, such as surface-enhanced Raman scattering (SERS) and enhancement of the luminescence of molecules situated near the surface of metallic nanostructures.

It has been established [1] that the local field enhancement effect is most significant near the SPR absorption bands of metallic nanoparticles. In turn, the spectral position of the SPR absorption bands is determined by the size of the nanoparticles, their shape and internal structure, and also the dielectric properties of the matrix in which they are embedded [2]. The near field distribution is also sensitive to all these parameters [3–7]. In this case, for example, in order to increase the intensity of Raman scattering by molecules situated near the surface of metallic nanoparticles, spectral overlap of the absorption bands of the selected molecules and the SPR absorption bands is of fundamental importance.

In order to determine the optimal conditions for resonance local field enhancement by metallic nanospheres, in this work we have studied the topology of the near field distribution for silver nanoparticles of different sizes; we have established the characteristic localization scales for the local field enhancement regions; and we have also studied the dependence of the attainable values of the local field enhancement factor on the sizes of the silver nanoparticles and the properties of the dielectric environment.

Calculation Method. We used Mie theory to determine the internal field and the field near the surface of a spherical particle. This method is based on expansion of all the fields (incident, scattered by particles, and internal) in vector spherical harmonics and subsequent numerical solution of the system of algebraic equations to determine the expansion coefficients [8–10]. We used our own version of a computer program which allows us to calculate the optical extinction, scattering, and absorption efficiency factors for the particles, and also the normalized amplitude of the elec-

*To whom correspondence should be addressed.

B. I. Stepanov Institute of Physics, National Academy of Sciences of Belarus, 68 prosp. Nezavisimosti, Minsk 220072; e-mail: ponyavina@imaph.bas-net.by. Translated from Zhurnal Prikladnoi Spektroskopii, Vol. 75, No. 6, pp. 831–837, November–December, 2008. Original article submitted June 20, 2008.

 0021-9037/08/7506-0832

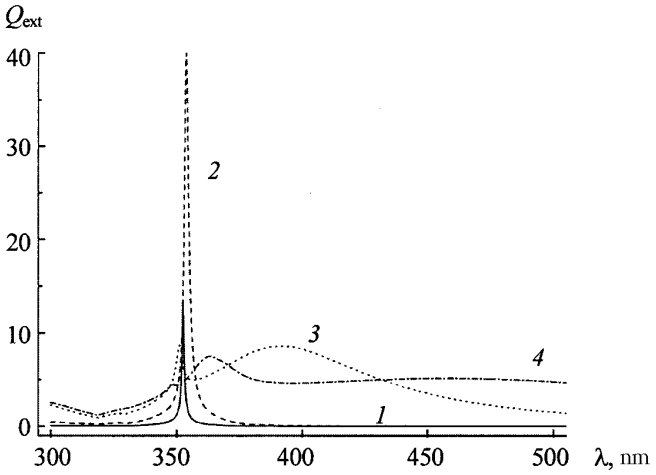

Fig. 1. Spectral dependences of the extinction efficiency factor for silver nanoparticles of radius: a = 2 nm (1), 10 nm (2), 50 nm (3), and 75 nm (4); refractive index of the matrix, n_0 = 1.

tric field strength both inside the particle and in the near field. For analysis of the near field distribution, we introduced the field enhancement factor $k = |E|/|E_0|$, where $|E|$ and $|E_0|$ are the local and incident field amplitudes. The analysis was performed for 4–150 nm silver nanospheres. The optical constants for silver were taken from [11]. The calculations were performed for radiation linearly polarized along the x axis with wavelength 400 nm, which corresponds to the maximum of the excitation spectrum for porphyrin molecules. To illustrate the shift of the surface plasmon resonance relative to the wavelength under consideration, Figure 1 shows the extinction spectra for silver nanoparticles of different sizes.

Numerical Experiment and Discussion of Results. In order to visualize the field distribution inside and outside the particle, we used two-dimensional ($2D$) diagrams drawn along the surface of cross sections passing through the center of the particle and perpendicular to the three axes of the rectangular coordinate system: cross section $A \perp x$, cross section $B \perp y$, cross section $C \perp z$.

Figure 2 shows the field distribution patterns for spherical nanoparticles of radii a = 2, 10, 50, and 75 nm, situated in a matrix with refractive index n_0 = 1. The field amplitude is specified by shades of gray, the intensity of which varies from black (amplitude equal to 0) to white, corresponding to a field amplitude of $3E_0$. We see that for the particle with the smallest radius (a = 2 nm), symmetry of the field patterns is characteristic both inside and outside the particle relative to all the planes of cross sections A, B, and C. The regions of the maximum field amplitude values ("hot spots") are mainly concentrated on the surface of the particle, near its diametrically opposed poles, along the polarization vector of the incident radiation. For the particle with a = 2 nm, the field value at the hot spots is equal to $5.4E_0$. As we move away from the surface of the particle, the field rapidly attenuates, and at distances greater than $2a$ from its center, the field amplitude everywhere is $<1.6E_0$.

The diagrams for the particle of radius a = 10 nm (Fig. 2b) are practically the same as the diagrams for the particle with a = 2 nm with respect to the nature of the spatial field distribution. The maximum attainable local field enhancement factor slightly increases and reaches a value of $5.6E_0$. For the particle of radius 50 nm (Fig. 2c), an even greater increase in the field amplitude at the hot spots is typical, reaching a value of $7.9E_0$, where the location of the hot spots themselves remains practically unchanged. However, the symmetry in the field distribution outside the particle, characteristic for small Rayleigh particles, is broken. The regions of significant local field enhancement are shifted toward the direction of the incident radiation. This shift is even more pronounced on further increase in the particle sizes, as demonstrated by the diagrams in Fig. 2d (cross sections A and B) for a particle of radius 75 nm. In this case, we also observe a shift in the two hot spot localization centers along the surface of the particle by a polar angle of $\approx 38^{\circ}$ compared with their position for a Rayleigh particle. The maximum field amplitude at the hot spots decreases in this case, and takes on a value of $5.5E_0$.

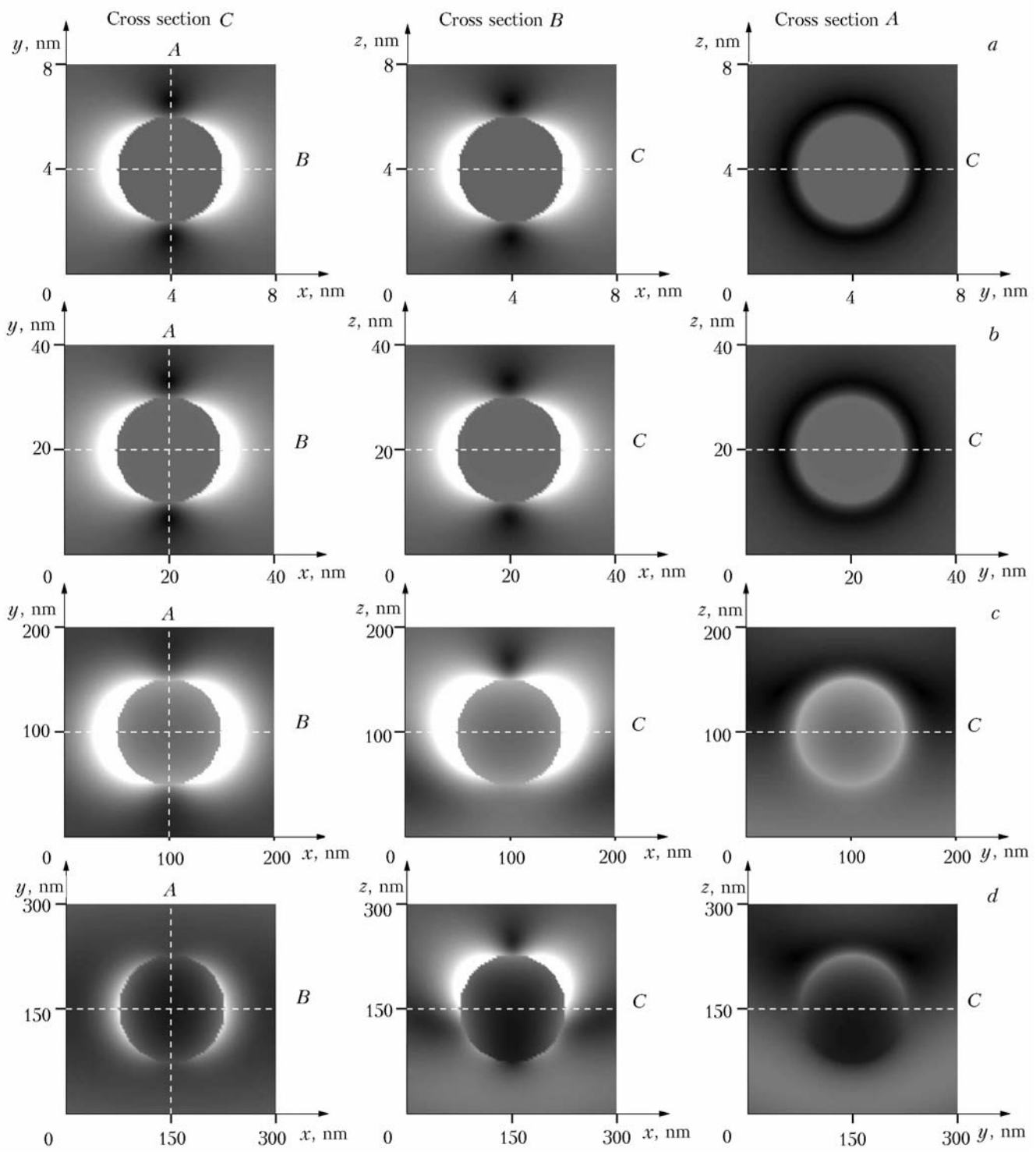

Fig. 2. 2*D* field distribution diagrams in planar cross sections *A*, *B*, *C* of silver nanoparticles of radius 2 nm (a), 10 nm (b), 50 nm (c), and 75 nm (d); wavelength of incident radiation, λ_0 = 400 nm; n_0 = 1.

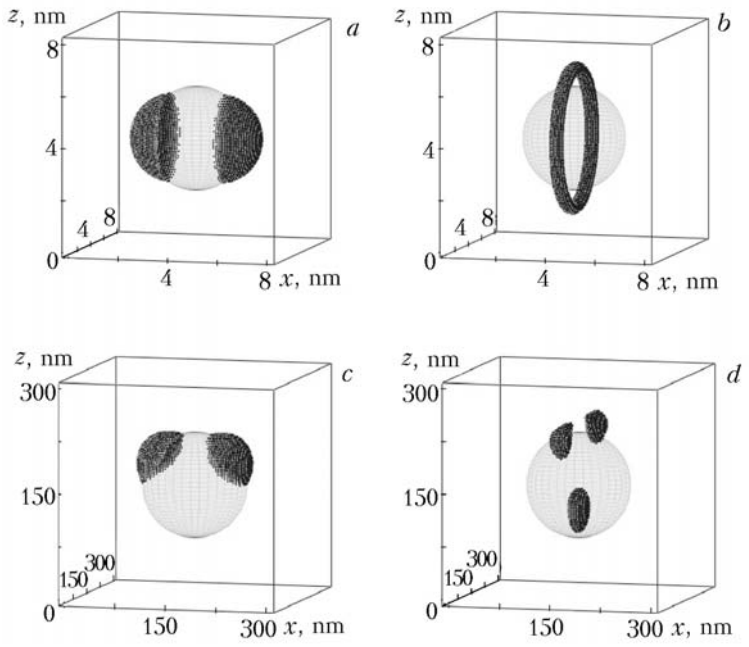

Fig. 3. 3D diagrams of spatial regions with field amplitudes: $>3E_0$ (a, c), $<0.3E_0$ (b, d); nanoparticle radius a = 2 nm (a, b) and 75 nm (c, d), n_0 = 1.

Figure 3 shows the spatial (3*D*) diagrams for particles with a = 2 and 75 nm. Using these diagrams, we can represent the spatial arrangement of the regions with values of the field amplitude filtered according to a certain criterion: $>3E_0$ and $<0.3E_0$. Each element of space satisfying one of the conditions is shown as a black point. Near the particle, besides regions with a high amplitude value, there are regions with field amplitude close to zero. Let us arbitrarily call them "cold spots". This region for particles with a = 2 nm has the shape of a ring with average radius ≈2.6 nm. The center of the ring coincides with the center of the spherical particle, while the plane of the ring is perpendicular to the line of polarization of the incident wave (Fig. 3b). As the particle radius increases, the hot spots move in the direction of propagation of the incident wave, always remaining outside the particle in the immediate vicinity of its surface (Fig. 3c). In this case, the field amplitude reaches the maximum values directly on the particle surface. The ring of low amplitudes breaks up as the radius increases, and outside the particle the regions of high and low amplitudes are adjacent (Fig. 3d).

Figure 4 shows the dependence of the maximum attainable local field enhancement factor k_{max} on the size of the metallic nanospheres for several values of the matrix refractive index. As we see, the general trend is a nonmonotonic dependence of k_{max} on the nanoparticle size, i.e., for each value of the refractive index of the matrix, we can determine the optimal radius at which the local field enhancement factor reaches the maximum value for the selected matrix and wavelength of the incident radiation. For example, for a matrix refractive index n = 1.3, the optimal radius is 21 nm; in this case, k_{max} = 23.1.

It is important to note that increasing the refractive index of the matrix from 1 to 1.45 leads to a shift of the optimal particle size a_0 toward lower values of the radius a. In this case, the higher the refractive index of the matrix, the higher the values of the absolute maximum kmax. For example, for a refractive index of the matrix n = 1.45, the optimal radius is 9.8 nm and k_{max} = 51.9. Further increase in n_0 leads to the appearance of several maxima on the $k_{max}(a)$ dependence, and the first maximum is gradually shifted toward larger particle sizes. The corresponding values of k_{max} decrease. Thus for n_0 = 1.6, a_0 = 30.2 nm, and k_{max} = 19.5.

Thus in the range of variation of the matrix refractive index from 1 to 1.75, we observe a nonmonotonic dependence of k_{max} on both the particle size and the refractive index of the matrix. This trend is illustrated in Fig. 5, on which we give the values of the enhancement coefficient for the field amplitude, calculated for variation in the particle radius and the refractive index of the matrix. We see that in the studied range of variation in the silver particle

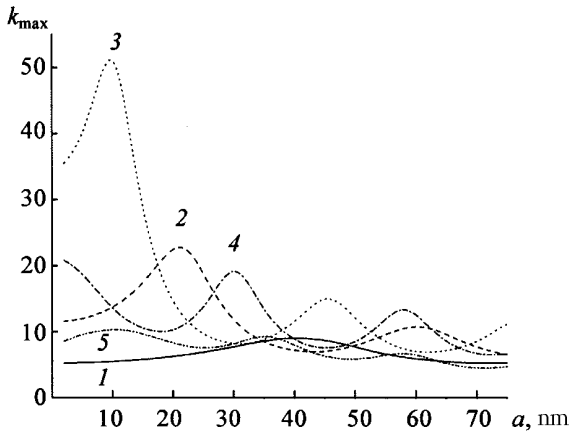

Fig. 4. Dependences of the maximum attainable local field enhancement factor vs. the silver nanoparticle radius (λ_0 = 400 nm, n_0 = 1.0 (1), 1.3 (2), 1.45 (3), 1.6 (4), 1.75 (5)).

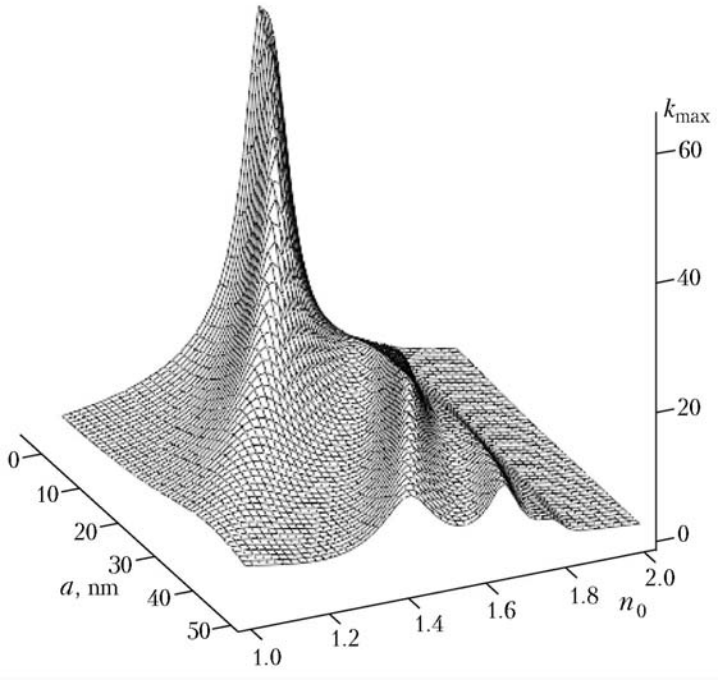

Fig. 5. Dependence of k_{max} on the nanoparticle radius and the refractive index of the matrix.

parameters: a = 2–75 nm and n_0 = 1–2, the peak of k_{max} = 63.7 is observed at a = 2 nm and n_0 = 1.5. Consequently, for each value of the matrix refractive index, there is an optimal nanoparticle radius, and conversely for each nanoparticle radius there is an optimal matrix refractive index. Thus in a matrix with refractive index 1.33, according to our calculations, the optimal choice for the nanoparticle radius is 19.2 nm. In this case, the enhancement factor is equal to 26.7.

It is important to note a certain correlation between the field amplitudes at the hot spots and the efficiencies of angle-integrated scattering and absorption of radiation. Thus for n_0 = 1, the maximum value of the field, equal to $9.2E_0$, is noted specifically for a particle of radius 41 nm, close to the radius 43 nm which corresponds to the plasmon

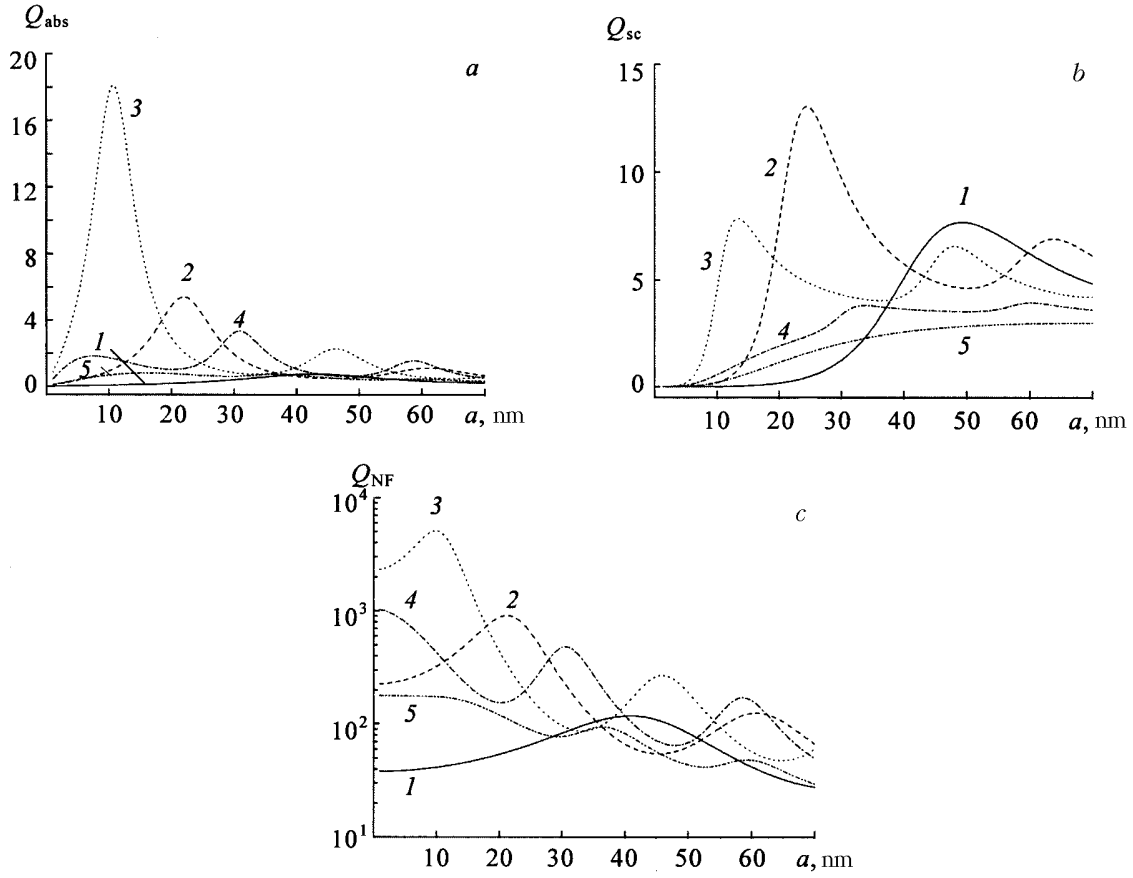

Fig. 6. Dependences of the absorption efficiency factor Q_{abs} (a), the far field scattering efficiency factor Q_{sc} (b), and the near field scattering efficiency factor (for $\xi = a$) Q_{NF} (c) vs. the nanoparticle radius: λ_0 = 400 nm, n_0 = 1 (1), 1.3 (2), 1.45 (3), 1.6 (4), 1.75 (5).

absorption maximum at the considered wavelength (see Fig. 6). For different values of the matrix refractive index, we show the absorption efficiency (Q_{abs}), the far field integrated scattering efficiency (Q_{sc}), and the near field integrated scattering efficiency (Q_{NF}) vs. the radius of a spherical particle.

Messinger [12] introduced the characteristic of the efficiency of conversion of an incident electromagnetic wave by a particle into scattered near field radiation, in analogy to the far field scattering efficiency:

$$Q_{NF} = \frac{\xi^2}{\pi a^2 I_0} \int_0^{2\pi} \int_0^{2\pi} \mathbf{E}_s \mathbf{E}_s^* \sin\theta d\theta d\varphi \,|_{\xi=a},$$

where $\mathbf{E}_s$ is the electric field vector of the scattered wave in the near field; ξ is the radius of the spherical surface over which the integration is done (in this case, the surface of a particle of radius a); I_0 is the intensity of the incident light.

As we see, this definition is different from the definitions of the efficiency factors introduced directly in Lorenz–Mie theory (where under the integral signs, we see the electromagnetic energy fluxes through a unit area of a sphere of radius a) in that the near field characteristic Q_{NF} provides a measure of the overall intensity of the scattered radiation along the sphere of integration rather than a characteristic of the total flux. In other words, the value of Q_{NF} describes how great the local field intensification is along the sphere of radius ξ, regardless of the mutual orientation of the normal vector to the surface of integration and the scattered electric field vector ($\mathbf{E}_s$) and magnetic field vector

($\mathbf{H}_s$). We should note that the value of Q_{NF} calculated for increasing ξ asymptotically approaches the value of Q_{sc} [12, 13].

Comparative analysis of the near field and far field scattering factors (Fig. 6) for uniform metallic nanospheres in different matrices indicates that the value of Q_{NF} may exceed Q_{sc} by more than a factor of 10, attaining the maximum absolute value for silver nanospheres in a matrix with $n_0 = 1.5$. Furthermore, for a constant value of the refractive index of the matrix, the value of Q_{NF} reaches a maximum value for smaller particle sizes than for Q_{sc}. From comparison of Figs. 4 and 6 we see that the best correspondence between the optimal sizes for attaining the maximum values for the integrated and local field characteristics is observed when using Q_{NF} or Q_{abs}.

Conclusion. The results obtained may be useful in choosing the optimal conditions for realization of surface-enhanced effects, such as luminescence and Raman enhancement effects.

A nonmonotonic dependence of the maximum attainable local field enhancement factor on the silver nanoparticle size is observed. For example, for silver nanoparticles of spherical shape in air, the optimal size is $a = 41$ nm. Furthermore, a nonmonotonic dependence of the optimal nanoparticle size and the maximum attainable local field enhancement factor on the refractive index of the surrounding medium has been established, which we also need to take into account when constructing active elements for surface-enhanced Raman scattering. We have shown that a good practical guide for determining the optimal nanoparticle sizes is analysis of the change in the absorption spectra of the nanoparticles as their sizes vary. This is based on the identified correlation between the optimal nanosphere sizes for the maximum attainable local field enhancement factor and the absorption efficiency factor.

REFERENCES

1. D. A. Stuart, A. J. Haes, C. R. Yonzon, et al., *IEE Proc. Nanobiotechnol.*, **152**, 13–32 (2005).
2. C. F. Boren and D. R. Huffman, *Absorption and Scattering of Light by Small Particles* [in Russian], Mir, Moscow (1986).
3. A. Pack, M. Hietschold, and R. Wannemacher, *Opt. Commun.*, **194**, 277–287 (2001).
4. M. Quinten, *Appl. Phys. B*, **73**, 245–256 (2001).
5. T. Jensen, L. Kelly, A. Lazaridies, and G. Schatz, *J. Cluster Sci.*, **10**, 295–297 (1999).
6. V. A. Shubin, W. Kim, V. P. Safonov, A. K. Sarychev, R. L. Armstrong, and V. M. Shalaev, *J. Lightwave Technology*, **17**, 2183–2218 (1999).
7. A. Ivinskaya, R. Dynich, and A. Ponyavina, *Physics, Chemistry and Applications of Nanostructures: Rev. and Short Notes to NANOMEETING-2005*, Minsk, 24–27 May 2005, World Scientific, Singapore (2005), pp. 247–250.
8. H. C. van de Hulst, *Light Scattering by Small Particles* [Russian translation], Inostr. Lit., Moscow (1961).
9. M. I. Mishchenko, L. D. Travis, and A. Lacis, Scattering, *Absorption and Emission of Light by Small Particles*, University Press, Cambridge (2002).
10. L. G. Astaf'eva, V. A. Babenko, and V. A. Kuzmin, *Electromagnetic Scattering in Disperse Media: Inhomogeneous and Anisotropic Particles*, Springer-Prexis, Berlin (2003).
11. P. B. Johnson and R. W. Christy, *Phys. Rev. B*, **12**, 4370–4387 (1972).
12. B. J. Messinger, K. U. von Raben, R. K. Chang, and P. W. Barber, *Phys. Rev. B*, **24**, 649–657 (1981).
13. K. L. Kelly, E. Coronado, L. L. Zhao, and G. C. Schatz, *J. Phys. Chem. B*, **107**, 668–677 (2003).